JOURNAL OF GEOPHYSICAL RESEARCH, VOL. 100, NO. C3, PAGES 4985–4993, MARCH 15, 1995

Runup kinematics on a natural beach

K.T. Holland
College of Oceanic and Atmospheric Sciences, Oregon State University, Corvallis

B. Raubenheimer and R.T. Guza
Scripps Institution of Oceanography, University of California, La Jolla

R.A. Holman
College of Oceanic and Atmospheric Sciences, Oregon State University, Corvallis

Abstract. Runup kinematics on a gently sloping natural beach are examined with detailed measurements from video images, resistance wires deployed at five elevations (between 5 and 25 cm) above and parallel to the beach face, and pressure sensors located in the inner surf zone. As suggested in a previous study comparing a single-level resistance wire and manually digitized films, runup measurements are sensitive to the sensor elevation above the bed, owing to the elongated shape of the runup tongue. The measured mean runup elevation (setup) and vertical excursion increase as the sensor elevation decreases, with the video-based runup estimates having the maximum means and variances. For the six data runs the average ratios of the video-based setup and significant runup excursion to estimates based on wires elevated 15 cm above the bed are 2.7 and 1.5, respectively. These trends, combined with the high coherence and small phase difference between the video and the lowest wire, demonstrate that the video-based estimates correspond to a very near-bed (less than a few centimeters elevation) wire measurement. The measured increase in runup excursion with decreasing sensor elevation and the cross-shore variation in the amplitudes of pressure fluctuations at infragravity frequencies, are consistent with the theory for linear, inviscid, normally incident standing waves. For example, valleys in the pressure spectra occur at approximately the predicted standing wave nodal frequencies. Also in accord with small-amplitude wave theory, observed swash excursions are nearly identical to pressure fluctuations at the location of the measured runup mean (for pressure sensors located seaward of the most offshore bed-level rundown). However, at very low frequencies, where reflection is typically assumed complete and dissipation negligible, the observed, near-bed swash magnitudes are overamplified relative to a best fit of the linear standing wave model based on the amplitude and phase of the seaward observations.

1. Introduction

Wave runup is loosely defined as the location of the moving point of beach-ocean intersection and is typically expressed in terms of its vertical excursion. Simple models [*Miche*, 1951] assume that runup oscillations represent the standing component of the incident wave field because the progressive component decays through dissipation to zero amplitude at the shoreline. Field studies confirm that runup spectra at infragravity band frequencies are often dominated by waves with a standing structure in the cross-shore direction [*Suhayda*, 1974; *Huntley*, 1976; *Guza and Thornton*, 1985] (and many others).

Holman and Guza [1984] (hereafter HG84) compared runup measured using manually digitized photographic films (visually estimated to sample a mean depth of 0.5 cm) with runup measured with resistance wire sensors elevated either 3 or 5 cm above the bed. Although spectral shapes were generally similar, substantial differences were found in the runup mean and variance and were attributed to thin tongues of runup sensed by the photographic technique, but not by the elevated wire. Therefore variations in runup sensor elevation could greatly affect estimates of surf zone infragravity wave motions based on runup measurements.

We present observations of runup on a natural beach which further define variations in runup kinematics as a function of sensor elevation. These detailed observations include runup from a newly developed video image processing technique and from a stacked array of resistance wire sensors deployed from 5 to 25 cm above the bed and sea surface elevation inferred from a cross-shore transect of pressure sensors in the inner surf zone. The experiment (described in section 2) results further illustrate the sensitivity of runup measurements to sensor elevation suggested by HG84 (section 3). We chose to explain these observations using theory for linear, inviscid, normally incident standing waves (section 4). For the most part, the standing wave theory serves as an excellent description of our observations. However, at low infragravity frequencies the near-bed swash excursions are larger than is expected based on the offshore standing wave structure and linear theory. The implications of these findings are discussed in section 5.

Paper number 94JC02664.
0148-0227/95/94JC-02664$05.00

2. Methods

Data were collected at Scripps Beach, California, from June 26–29, 1989. This fine-grained (mean diameter roughly 0.2 mm) sandy beach has a concave-up profile (Figure 1) with an approximate offshore slope of 0.01. Best fit foreshore slopes β over the region between maximum runup and minimum rundown varied between 0.030 and 0.043 (Table 1). Changes between consecutive daily profiles were small, typically about 5 cm in the swash region, so profile changes during the data runs were assumed negligible. Runup was measured with five resistance wire sensors (each similar to the single elevation sensor described by *Guza and Thornton* [1982]) stacked above the bed at elevations $\delta = 5$, 10, 15, 20, and 25 cm. These sensors are denoted R5, R10, ... R25. The 1-cm diameter rods supporting the 60-m long wires had no visible influence on the measured wave runup. Wires at each elevation measured the cross-shore location shoreward of which the water depth was less than the appropriate δ value. The horizontal resolution of the wires was less than 1 cm. The vertical runup component relative to a known datum was calculated using the beach profile $h(x)$ and the individual sensor height. Pressure sensors were located at various positions along the transect and are denoted by their cross-shore coordinate (i.e., P108 is located at offshore coordinate 108 m, Figure 1).

Table 1. Data Summary

Run	Date	Time, UT	Duration, hours	$\bar{\eta}$, cm	H_s, cm	R_{sR0}, cm	β
1326	June 26, 1989	1355	1.3	60	64	60	0.043
1327	June 27, 1989	1315	1.2	32	87	62	0.041
1228	June 28, 1989	1200	1.0	–18	82	40	0.030
1428	June 28, 1989	1408	0.9	30	82	47	0.039
1229	June 29, 1989	1250	1.5	–9	59	39	0.035
1429	June 29, 1989	1451	1.2	35	58	43	0.040

Abbreviations are $\bar{\eta}$, still water level; H_s, significant wave height; R_{sR0}, significant vertical runup excursion at RO; and β, best fit foreshore slopes.

Runup was also measured with video cameras overlooking the runup gauge transect, following an extension of the method outlined by [*Aagaard and Holm*, 1989]. Using the known geometric transformation between ground and image coordinates (resolved to within 1 cm vertically), the light intensity of each picture element (pixel) in the cross-shore transect was digitized. Plate 1 is a "timestack" of pixel intensities showing temporal and spatial runup variations. The runup position at each video sample

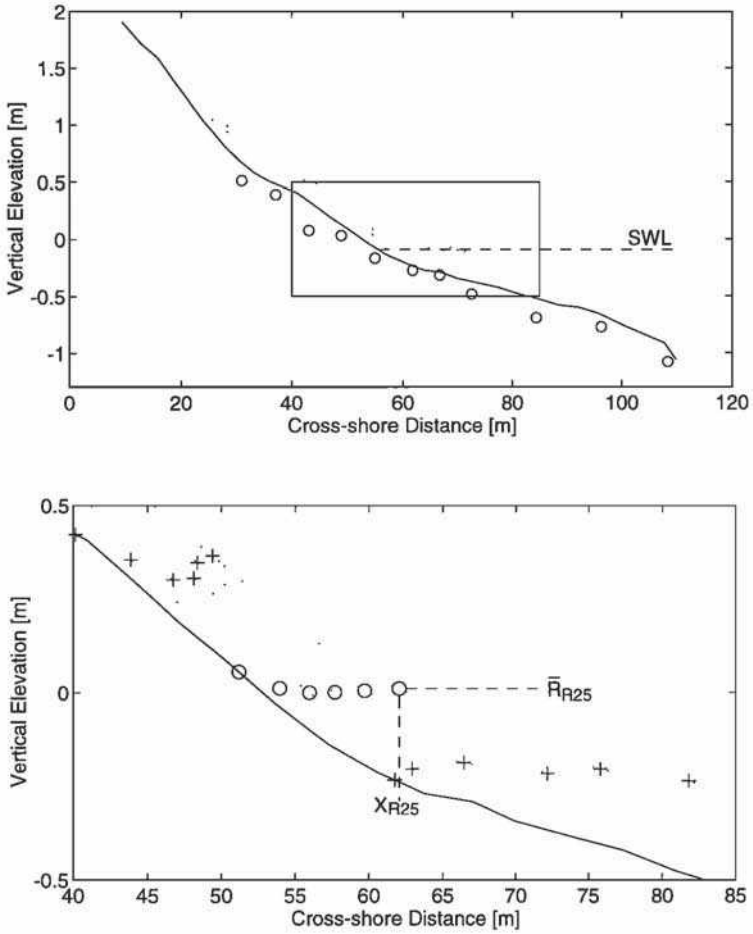

Figure 1. (top) June 29 beach profile with runup wires represented by dotted lines and the (buried) pressure sensors indicated by circles. Still water level from the tide gauge is shown by the dashed line. (bottom) Inset showing the maximum uprush and minimum rundown locations (pluses) and the mean vertical runup, $\bar{R}_{R\delta}$ (circles), measured by each runup sensor. Mean cross-shore runup sensor locations $X_{R\delta}$ are defined by the mean vertical runup elevation.

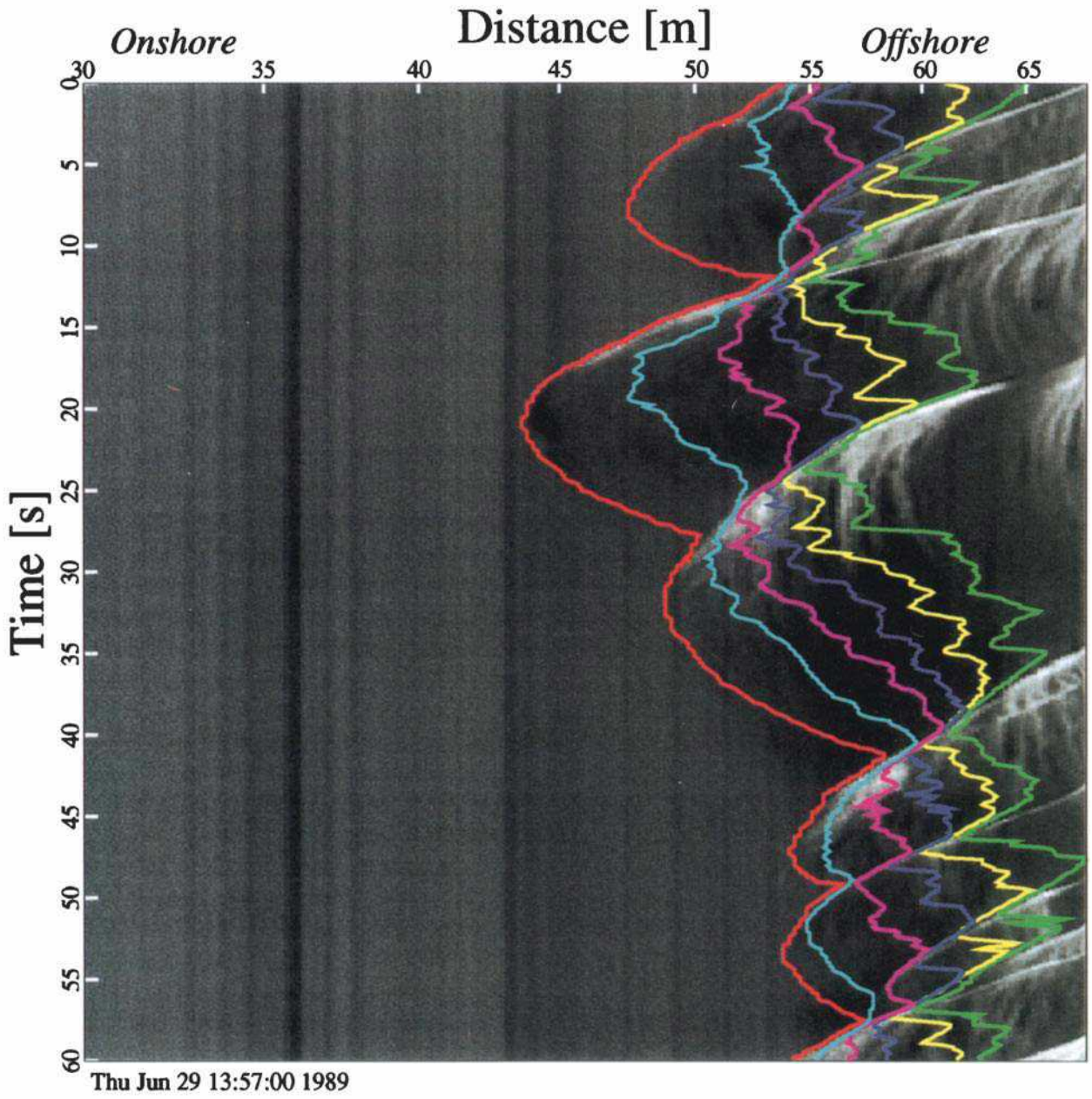

Plate 1. Video timestack for the 1229 run showing runup as a function of sensor elevation δ. Intensity patterns vary with time (down the page) and with cross-shore position (across the page). Line colors indicate the runup location at the various sensor elevations above the bed as follows: red (0 cm), cyan (5 cm), magenta (10 cm), blue (15 cm), yellow (20 cm), and green (25 cm).

time is the most landward identifiable edge (i.e., intensity gradient). The following results suggest a video sampling depth of less than a very few centimeters, consistent with the rough visual estimate of 0.5 cm (HG84). For this reason, the video will subsequently be referred to as a "bed-level" sensor and will be denoted as R0. HG84 discuss the logistical problems and advantages and disadvantages of the video and wire measurement techniques.

Video and wire runup measurements, superimposed on the timestack, (Plate 1) overlap when the leading edge of the uprush is a steep faced bore with height exceeding the elevation of the highest wire but are displaced and roughly parallel when the runup or rundown has an elongated tongue shape. As the sensor elevation δ decreases, the measured uprush extends farther landward, the downrush begins later, and the magnitude of high-frequency fluctuations appears to decrease relative to low-frequency fluctuations. The measured swash oscillations are obviously influenced by δ.

Six data runs were collected over a 4-day period with an 8-Hz sampling frequency and record lengths varying from 50 to 90 min. The time series were quadratically detrended to suppress tidal fluctuations. In the 1326 run (run names correspond to the starting hour and date of each data record), R5 and R20 were not usable because of kelp entangled in the wires. As part of an ongoing monitoring program [*Seymour et al.*, 1985], incident waves were measured every 6 hours in 7 m depth, a few hundred meters offshore and alongshore of the runup measurements. The spectral peak was typically 0.1 Hz, and significant wave heights H_s ranged between approximately 60 and 90 cm (Table 1). The

still water level $\bar{\eta}$ relative to a mean sea level datum was estimated from a nearby tide gage outside the surf zone.

3. Runup Statistics

Figure 2 shows the dependence of the measured setup elevation (the superelevation of the mean vertical runup level $\bar{R}$ above the offshore still water level) and significant vertical runup excursion R_s (calculated as $4s$, where s^2 is the total variance of vertical runup fluctuations about the mean) on δ. Consistent with the time series shown in Plate 1, both the setup and the significant runup excursion (each normalized by the offshore significant wave height) increase with decreasing δ. In most cases, owing to the sensitivity of thin tongues to runup, the increases are largest for sensor elevations less than 10 cm. For example, the average normalized setup from R0 (the video) is approximately 3 times that measured by R15 (the middle wire), which is itself about 1.5 times the setup on the uppermost wire, R25 (Figure 2a). Similarly, the significant runup excursions at R0 are roughly a factor of 1.5 greater than those at R15, whereas R_s estimates from the three highest sensors are quite similar.

Runup spectra (representative examples are shown in Figure 3a) have maximum power at infragravity frequencies (less than 0.05 Hz), typical of low slope beaches. The increase in runup excursion with decreasing δ (Figure 2b) is due to a monotonic increase in infragravity energy. Nonmonotonic changes in higher-frequency energy have little impact on the total variance. Coherence and phase differences between R0 and all higher wires are shown for the 1229 run in Figures 3b and 3c. At frequencies below 0.02 Hz the squared coherence is high (>0.6) and the phase difference is nearly zero. With increasing frequency and wire elevation the coherence drops and phase differences with R0 increase (wires lead R0). The highest coherence and smallest phase differences are between R0 and R5. The trends (with δ) of the runup statistics (Figure 2) and of the coherence and phase (Figures 3b, and 3c) appear consistent with a δ_{R0} of less than a few centimeters. There is no indication that the video differs substantially from a very near bed wire.

4. Comparison With Linear Theory

At approximately 0.035 Hz (a spectral valley for R25) the coherence between R0 and R25 drops and the phase jumps about 180° (Figures 3a, 3b, and 3c). The R0–R20 cross spectrum has similar characteristics. Coherence drops and phase jumps between R0 and the upper wires (also seen in the 1228 run) are similar to those observed between runup and inner surf zone pressure measurements and attributed to standing wave nodal structure (Suhayda [1974] and many others). The very similar spectra, high coherence, and the near-zero phase difference between P62 and R25 (X_{R25} = 62.2 m) confirm that runup measured with wires elevated above the bed can closely approximate those from collocated pressure sensors (Figure 4). Note that the P62-R0 pair has a phase jump and drop in coherence very similar to that between R25 and R0. This similarity between runup measured with the upper wire and sea surface elevation measured with a fixed pressure sensor (located at the mean runup) is expected for small-amplitude waves, because the horizontal posi-

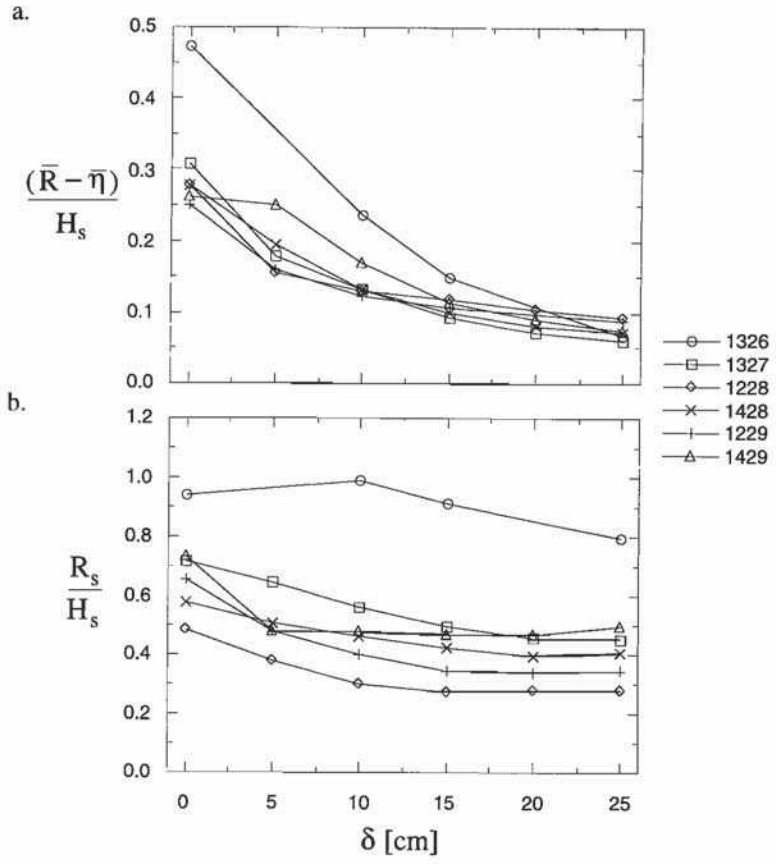

Figure 2. (a) Normalized mean vertical runup relative to the still water level at a nearby tide gauge, i.e., setup, $(\bar{R}-\bar{\eta})/H_s$ and (b) normalized significant runup excursion (R_s/H_s) versus δ. All six data runs are shown.

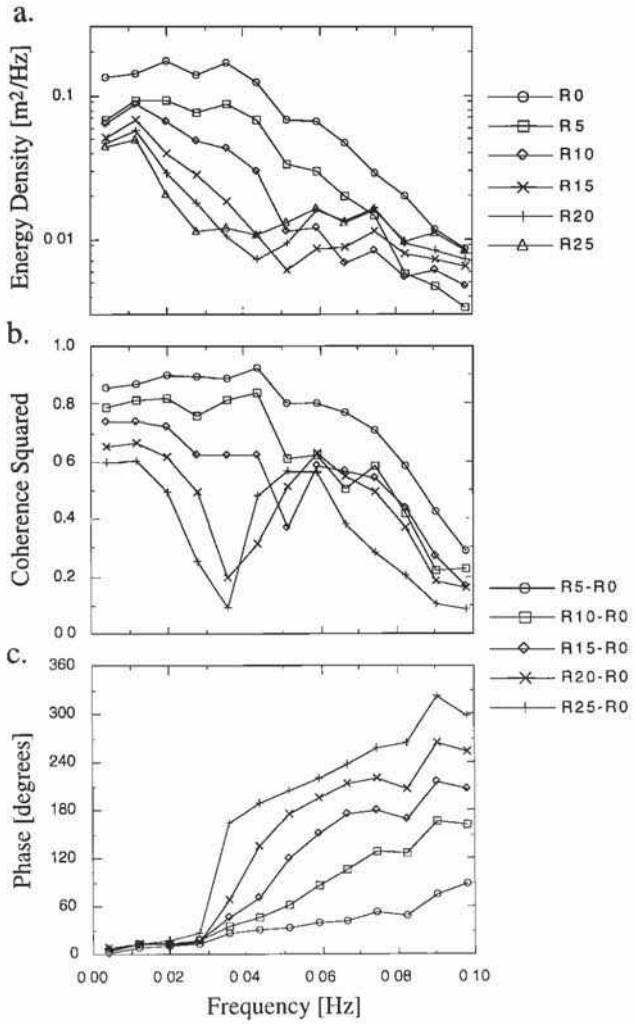

Figure 3. For the 1229 run, (a) spectra for all runup sensors, (b) squared coherence, and (c) phase for the 1229 run as a function of δ and frequency. Coherence and phase estimates are between R0 and higher sensors as indicated. The 95% significant squared coherence level (80 degrees of freedom) is 0.074.

tion of the runup never varies substantially from its mean cross-shore position $X_{R\delta}$. The coherence drop between R25 and P62 that occurs with no corresponding, consistent change in phase suggests that both sensors are located at a cross-shore node for 0.035 Hz. Results are similar (not shown) for other approximately collocated wires and pressure sensors when the cross-shore mean runup location is seaward of the most offshore bed-level rundown. Spectra from a sensor at lower δ (such as R0 or R5) and its collocated pressure sensor cannot be similarly compared, because the pressure sensor is located landward of the most offshore bed-level rundown and therefore only records a partial swash cycle. During extreme rundown the collocated pressure sensor measures the roughly constant pressure of the saturated sand overburden, whereas the runup sensor records the entire swash cycle.

The coherence and phase observations appear at least qualitatively consistent with our expectations for standing waves. To more rigorously test this hypothesis, the data were compared to the theoretical cross-shore structures of small amplitude, shallow water waves fully reflected at the shoreline. Assuming surface elevations of the form $\eta = a_s \cos(\sigma t)$, where σ is the radial frequency and a_s is the wave amplitude at the shoreline, predicted standing wave magnitudes, $|\phi(x)|$ and the corresponding phase structures were calculated for the measured bathymetry seaward of the still water shoreline. Following *Holman and Bowen* [1979], we numerically solved the linear shallow water equation,

$$\frac{\sigma^2}{g}\phi + \frac{d}{dx}\left(h\frac{d\phi}{dx}\right) = 0$$

where $h(x)$ is the water depth below the still water level and g is the gravitational acceleration. The two shoreline boundary conditions were determined by defining $\phi(x=0) = 1$, expanding $h(x)$ and $\phi(x)$ as power series and equating coefficients of like powers. Possible setup effects were neglected. Although the above model applies only to leaky waves, it can be shown that the amplitude decay scale, $\partial\phi/\partial x$ at $h=0$, is the same for all linear free waves and is, for near planar foreshores, approximately $-\sigma^2/(g\beta)$ where β is the mean profile slope in the vicinity of the shoreline.

Figure 5 shows the measured cross-shore variation in wave magnitude and phase for run 1229 at frequency 0.035 Hz. The two predictions shown are relative to the measured shoreline magnitudes of R0 and R5. Although there appears to be some

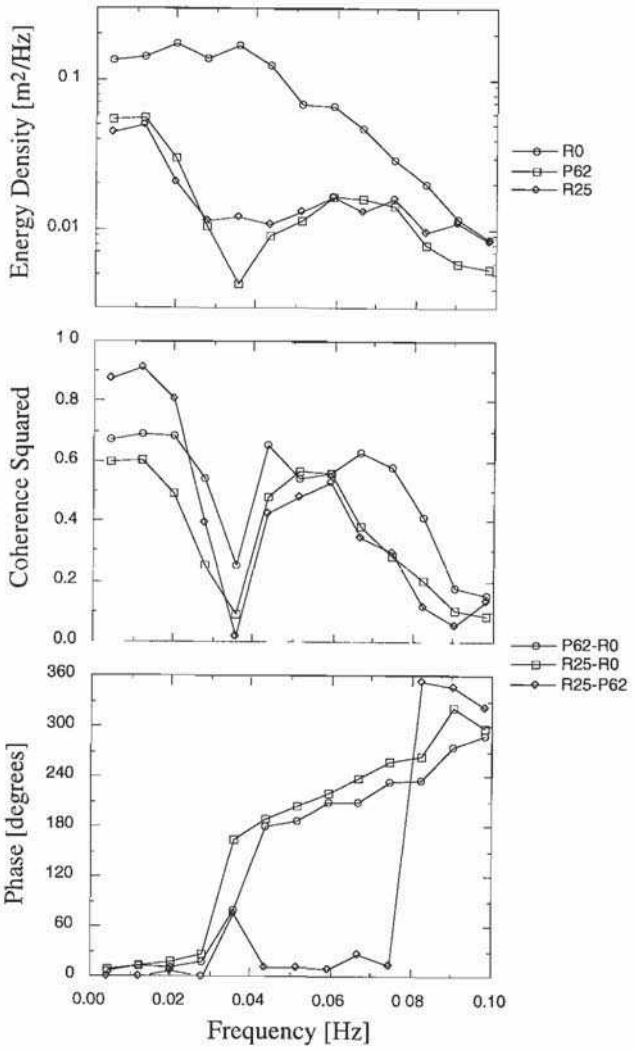

Figure 4. Cross-spectra between R0, R25, and the pressure sensor (P62) collocated (see text) with R25 for the 1229 run.

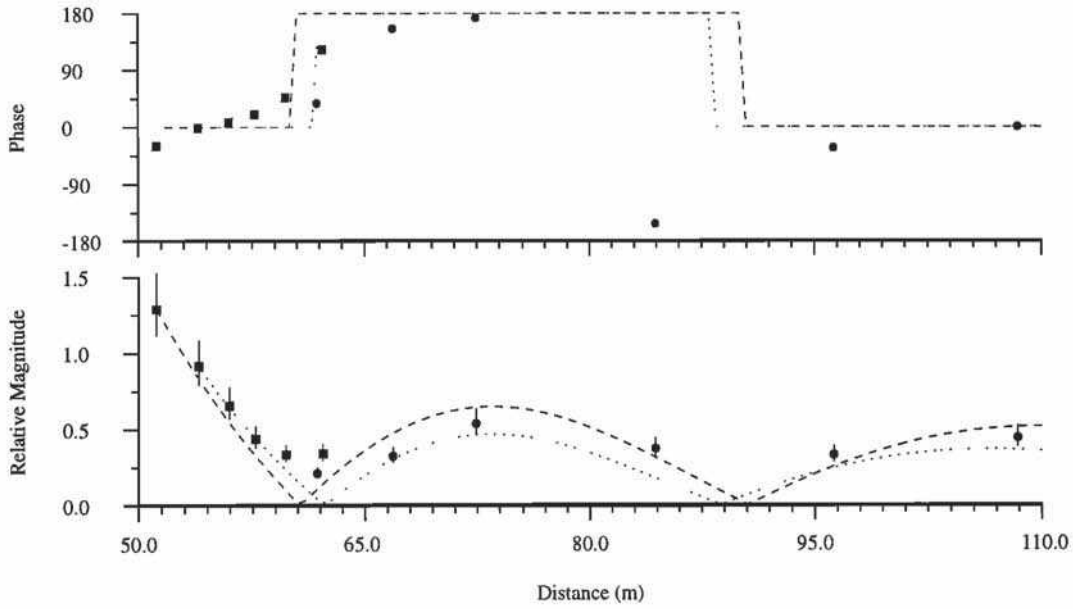

Figure 5. Cross-shore magnitude and phase structures for frequency 0.035 Hz for the 1229 run. Magnitude estimates were calculated within a frequency bandwidth of 0.001 Hz. Phases are shown relative to the phase at sensor P108. Observations from runup sensors (squares) and pressure sensors (circles) are compared with linear standing wave theory using the shoreline amplitude and location of R0 (dashed line) and R5 (dotted line). Runup observations are shown at the mean cross-shore location of each sensor $X_{R\delta}$. Vertical bars indicate 95% confidence limits.

residual progressive energy (indicated by the ramplike phase variation), the observed magnitudes and phases compare reasonably well with the linear theory predictions for a normally incident standing wave. The general agreement between theory and observations strongly supports the standing wave interpretation, as suggested in previous studies which used a single runup wire and offshore pressure gauges or current meters. Note, however, that in the present results which use runup measurements at multiple sensor elevations, the decrease in relative wave magnitude with increased runup sensor elevation is also well predicted.

The comparison of model and data in Figure 5 could be made more diagnostic if the magnitude and phase information could be combined to produce a single, signed amplitude plot. In the present paper this was accomplished in two steps. First the cross-shore structure of the data was quantified using frequency domain, complex empirical orthogonal function (EOF) decomposition of the cross-spectral matrix between all instrument pairs [*Wallace and Dickinson*, 1972]. Note that a priori selection of a reference sensor for phase calculations is not required (phase data from Figure 5 is based on only the last column of the cross-spectral matrix). Complex eigenvectors can also be expressed in terms of real and imaginary components. If the vector elements are plotted on the real-imaginary plane, the pattern of points is diagnostic of the associated wave type. The points for a purely progressive wave in constant depth will define a circle (or the arc of a circle if the array is shorter than a wavelength), while for a primarily standing wave the points will be distributed along a principle axis. Thus the final step for calculation of a signed amplitude function $A(x)$ for such a standing wave is the projection of the vector elements onto the principle axis. A qualitative measure of the relevance of the standing wave assumption is given by the percentage of variance (in the real-imaginary plane) explained by that projection. Amplitude distortions introduced by assuming the magnitude structure is purely real (i.e., neglect of imaginary components) are estimated to be less than 10% for frequencies less than or equal to 0.035 Hz.

To compare observed, signed amplitude structures, $A(x)$, with the linear standing wave model $\hat{a}_s\phi(x-\hat{x}_0)$, the best fit shoreline amplitude $\hat{a}_s$ and shoreline position $\hat{x}_0$ were estimated using a least squares approach (for each frequency the sum of squares error was found for a range of choices of $\hat{x}_0$ with the best fit values being associated with minimum error). At low frequencies for which there is little cross-shore structure, the error is only weakly sensitive to $\hat{x}_0$. At higher frequencies, where the cross-shore structure is more complex, the estimates of $\hat{x}_0$ are well constrained. A typical error bar for $\hat{x}_0$ (based on the sum of squares error being within 50% of its minimum value) is approximately ±2.5 m.

For run 1229 at 0.035 Hz the magnitude and phase (Figures 6a and 6b) of the first (dominant) complex eigenvector, which explains approximately 85% of the variance in this band, is quite similar to the measured magnitude structure (Figure 5) and consistent with the standing wave interpretation. The observed cross-shore structure of normalized signed amplitudes $[\tilde{\phi}_{obs}(x) = A(x)/\hat{a}_s]$ closely matches the standing wave model (Figure 6c). Note that the location of the first node at approximately 62 m corresponds to the mean cross-shore location of R25, consistent with the spectral valley and phase jump shown in Figures 4 and 5. Runup observations landward of the best fit shoreline cannot be explained in terms of the linear model.

Figure 7 shows the observed normalized amplitude structure, $\tilde{\phi}_{obs}(x)$, and the corresponding best fit linear solution $\phi(x)$ for three frequencies from run 1327. Measured and predicted phase structures are also shown for comparison. For each frequency the linear standing wave model agrees very well with the observed signed amplitude structure over most of the array despite the drift in phase (Figure 7, bottom) that appears related to a mix of some progressive energy with the standing motion. However, as δ decreases, discrepancies from the model are evident as overamplification (most obvious at lowest frequency), defined as

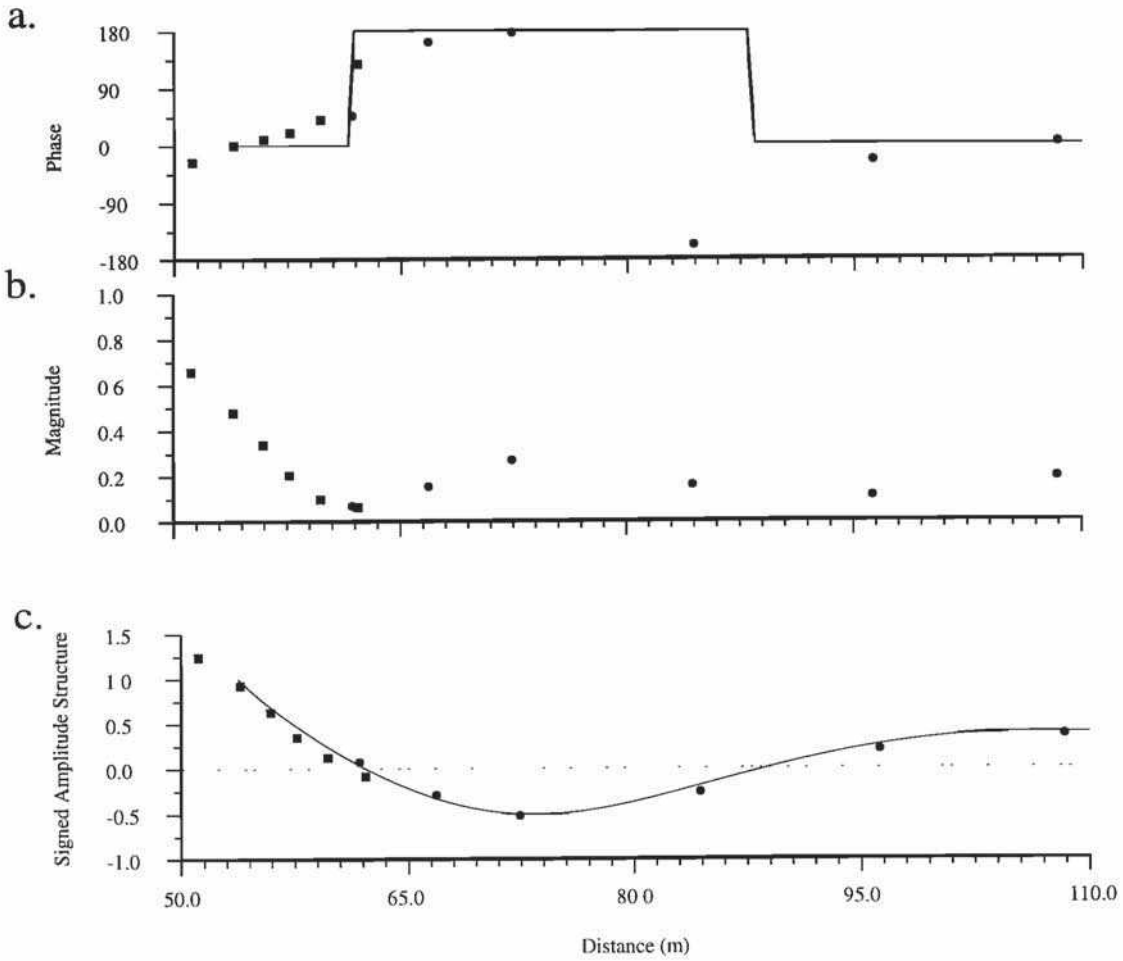

Figure 6. Complex empirical orthogonal function (EOF) decomposition of the cross-spectral matrix between all possible instrument pairs for frequency 0.035 Hz for the 1229 run. (a) Phase, (b) magnitude, and (c) normalized signed amplitudes (see text). The solid line is the best fit linear standing wave.

normalized observed amplitudes greater 1.0. Because the observed $\partial\tilde{\phi}/\partial x$ slopes of the runup sensors for frequencies 0.005 and 0.015 Hz (Figure 7, top and middle) are substantially steeper than the shoreline slope of the linear model, these overamplifications cannot be explained using linear theory in terms of either edge or leaky waves. In contrast, the near-bed overamplification in Figure 7, bottom, (and also Figure 6c) could possibly be due to the presence of low mode edge waves. Comparison of observed and predicted shoreline slopes for all runs indicates that nearbed signed amplitudes are, on average, incompatible with linear theory for frequencies below 0.02 Hz.

The consistent overamplification at low frequency and low δ is demonstrated by the average and range over the data runs of $\tilde{\phi}_{obs}(\delta)/\phi(\delta)$ (Figure 8). All EOFs explain at least 77% of the band variance (the average percentage is 84%). For sensors with mean positions landward of the estimated shoreline, $\phi(\delta)$ was set to 1.0. A general trend of decreasing overamplification with increasing δ is evident for the two lowest frequencies with the maximum ratios at R0. The largest observed signed amplitude was 2.5 times greater that expected using linear theory and occurred at lowest frequency. As frequency increases, however, the consistency of the trend disappears (Figure 8, bottom). These results indicate that overamplifications are largest at low infragravity frequencies and small δ.

5. Discussion

Sea surface and pressure fluctuations in the surf zone at infragravity wave frequencies where the nearshore wave field is primarily standing have previously been qualitatively well modeled using runup measurements and linear theory in both the lab and the field [*Suhayda*, 1974; *Guza and Bowen*, 1976] (and others). In these prior studies the mean shoreline location was defined as the horizontal position of the mean runup and the runup sensor elevation was implicitly assumed to be unimportant. However, our observations demonstrate that runup variance depends on δ.

At low infragravity frequencies ($f < 0.02$ Hz) we observed nearbed runup amplitudes substantially greater than that estimated from the nearshore wave field assuming linear, normally incident waves (Figure 8, top and middle). The influence of low mode edge waves has been suggested to explain similar results in previous data sets [*Guza and Thornton*, 1985; *Oltman-Shay and Guza*, 1987]. However, for these very low frequencies, neither leaky nor edge waves can explain the short cross-shore scale of the overamplifications. Yet these near-bed discrepancies from linear theory are not entirely unexpected. Nonlinear bore models for the runup of random waves have been developed and show marked differences from their linear counterparts (*Raubenheimer*

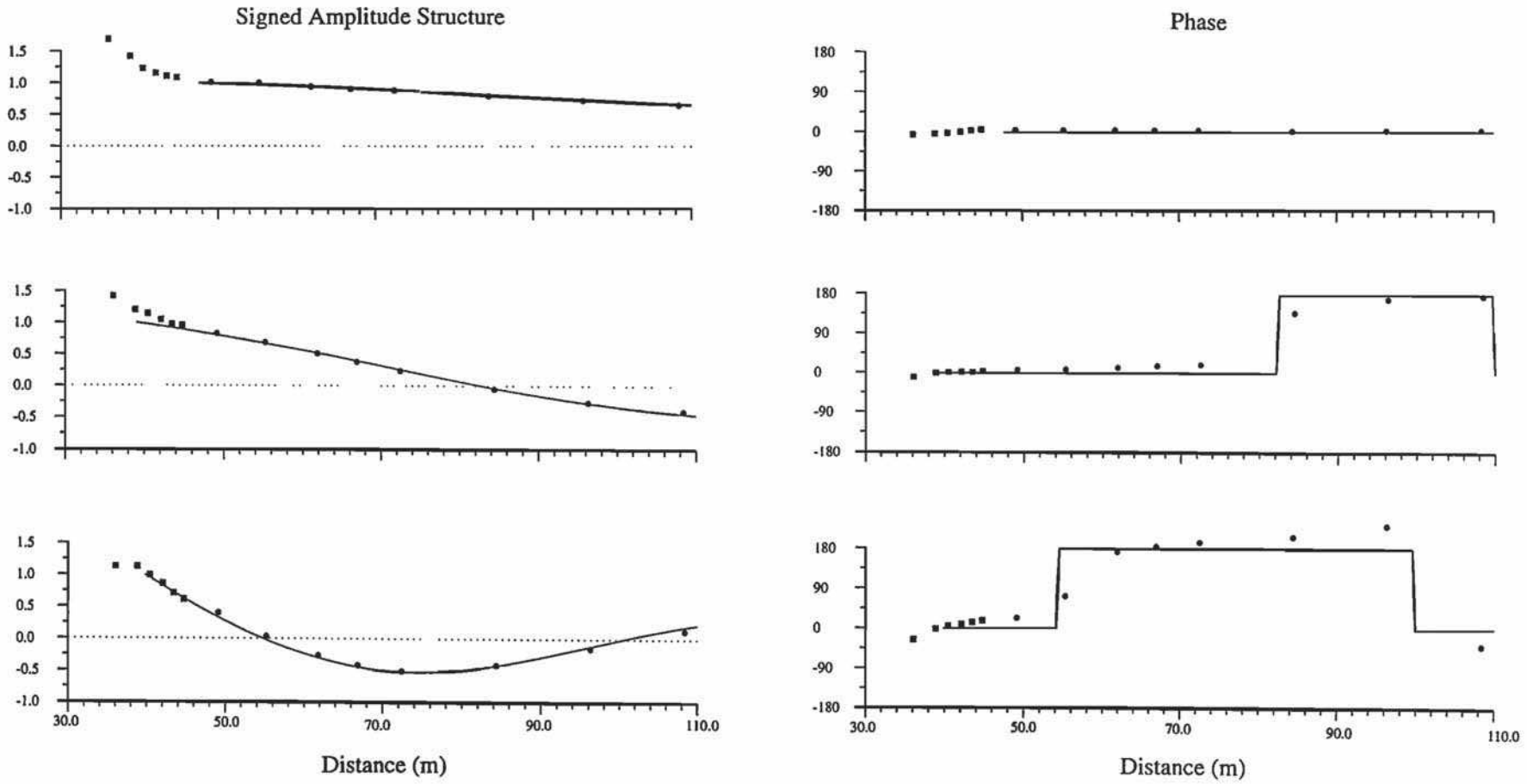

Figure 7. Normalized signed amplitude (left) and phase (right) for frequencies 0.005 (top), 0.015 (middle), and 0.030 (bottom) Hz for run 1327.

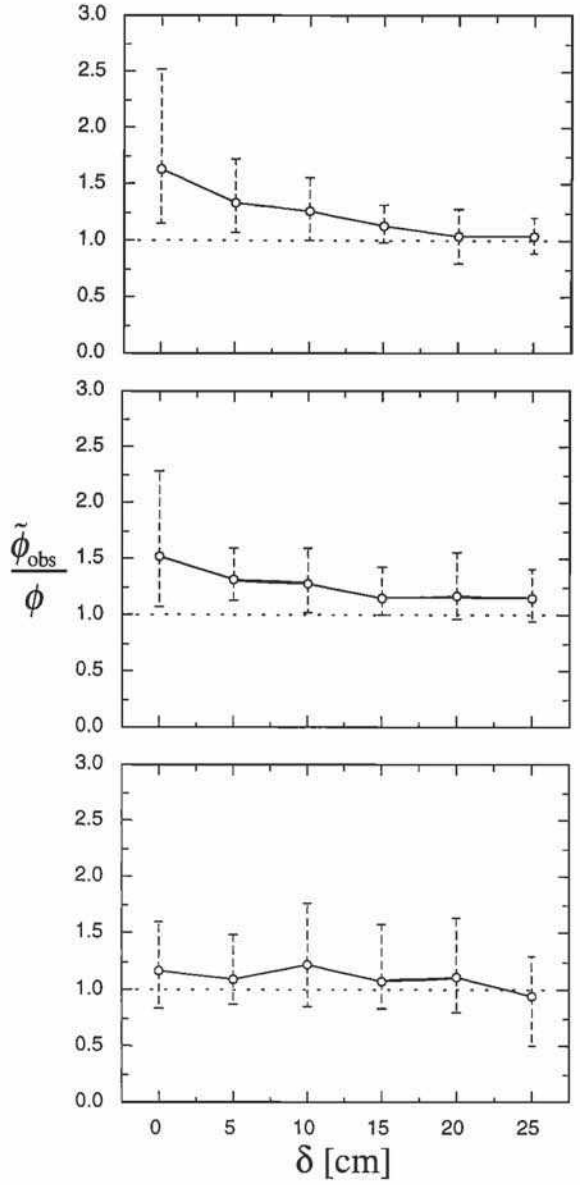

Figure 8. Ratio of observed to predicted signed amplitude structure for frequencies 0.005 (top), 0.015 (middle), and 0.030 (bottom) Hz as a function of δ. Circles are average values over six runs and vertical bars indicate observed ranges. Dotted line marks the maximum expected amplitude of 1.0.

et al. [1995] provide an example of a nonlinear model compared to these data). Further investigation may help clarify the cause of the overamplification and its dependence upon amplitude, beach slope, and/or some other variable in addition to wave frequency. In any case, users of linear theory predictions and reflection coefficient estimates that incorporate infragravity frequency runup measurements on low sloping beaches should be aware of the potential complexity of this region.

6. Conclusions

Results from a field experiment on a low slope beach demonstrate the dependence of runup kinematics on sensor elevation δ. Runup mean and excursion measured with resistance wire and video techniques increase with decreasing δ with the largest changes occurring for δ less than 10 cm. Energy levels in the infragravity frequency band, which dominate the runup spectra, increase with decreasing δ. No fundamental differences between video and wire runup sensor types are apparent. In addition, measured runup excursions at $\delta > 20$ cm appear equivalent to collocated pressure fluctuations, an observation in accord with linear small-amplitude wave theory. At low infragravity frequencies ($f < 0.02$ Hz), cross-shore standing wave patterns are observed, however, discrepancies are evident between the measured near-bed runup and linear standing waves. The magnitude of the discrepancies varies as a function of δ and of frequency, with the maximum overamplification of the swash measurements (approximately 2.5 times that predicted using linear theory) occurring at the lowest well-resolved frequency (0.005 Hz) and lowest δ.

Acknowledgments. K.T.H. and R.A.H. were supported by the U.S. Geological Survey, National Coastal Geology Program and the Office of Naval Research, Coastal Sciences Program. B.R. and R.T.G. were supported by the ONR (Coastal Sciences), the National Science Foundation (Physical Oceanography), an NDSEG Department of Defense graduate student fellowship, and the ONR (AASERT program). Staff from the Center for Coastal Studies, Scripps Institution of Oceanography, deployed and maintained the in situ instrumentation. The late Paul O'Neill operated and maintained the survey and video equipment.

References

Aagaard, T., and J. Holm, Digitization of wave run-up using video records, *J. Coastal Res.*, *5*(3), 547-551, 1989.

Guza, R. T., and A. J. Bowen, Resonant interactions for waves breaking on a beach, in *Proc Coastal Eng. Conf., Am. Soc. Civ. Eng., 15th* (1), 560-579, 1976.

Guza, R. T., and E. B. Thornton, Swash oscillations on a natural beach, *J. Geophys. Res.*, *87*(C1), 483-491, 1982.

Guza, R. T., and E. B. Thornton, Observations of surf beat, *J. Geophys. Res.*, *90*(C2), 3161-3172, 1985.

Holman, R. A., and A. J. Bowen, Edge waves on complex beach profiles, *J Geophys Res.*, *84*(C10), 6339-6346, 1979.

Holman, R. A., and R. T. Guza, Measuring run-up on a natural beach, *Coastal Eng.*, *8*, 129-140, 1984.

Huntley, D. A., Long-period waves on a natural beach, *J. Geophys. Res.*, *81*(36), 6441-6449, 1976.

Miche, R., Le pouvoir réfléchissant des ouvrages maritimes exposés à l'action de la houle, *Ann. Ponts Chaussees*, *121*, 285-319, 1951.

Oltman-Shay, J., and R. T. Guza, Infragravity edge wave observations on two California beaches, *J. Phys. Oceanogr.*, *17*(5), 644-663, 1987.

Raubenheimer, B., R. T. Guza, S. Elgar, and N. Kobayashi, Swash on a gently sloping beach, *J. Geophys. Res., in press*, 1995.

Seymour, R. J., M. H. Sessions, and D. Castel, Automated remote recording and analysis of coastal data, *J. Water. Port Coast. Ocean Eng.*, *111*(2), 388-400, 1985.

Suhayda, J. N., Standing waves on beaches, *J. Geophys. Res.*, *79*(21), 3065-3071, 1974.

Wallace, J. M., and R. E. Dickinson, Empirical orthogonal representation of time series in the frequency domain, I, Theoretical considerations, *J. Appl. Meteorol.*, *11*(6), 887-892, 1972.

K.T. Holland and R.A. Holman, College of Oceanic and Atmospheric Sciences, Oregon State University, Ocean Administration Building 104, Corvallis, OR 97331-5503. (e-mail: tholland@oce.orst.edu; holman@oce.orst.edu)

R.T. Guza and B. Raubenheimer, Center for Coastal Studies A-009, Scripps Institution of Oceanography, University of California, La Jolla, CA 92093-0209. (e-mail: rtg@coast.ucsd.edu; britt@coast.ucsd.edu)

(Received February 7, 1994; revised June 20, 1994; accepted September 16, 1994.)